Chinese Chemical Letters 37 (2026) 111980

Contents lists available at ScienceDirect

Chinese Chemical Letters

journal homepage: www.elsevier.com/locate/cclet

Selective nitrate photoreduction to ammonia on photo-induced halogen vacancies with promoted hydrogen atom transfer

Fuqiang Guo[a], Xian Shi[b], Xing'an Dong[a,*], Chunyu Li[a], Shanshan Xu[c], Wendong Zhang[c], Weidong Dai[d], Wenjie He[e], Xin Jin[a], Peng Yu[a,*], Fan Dong[d]

[a] College of Physics and Electronic Engineering, Chongqing Normal University, Chongqing 401331, China
[b] School of Chemistry and Environmental Engineering, Sichuan University of Science & Engineering, Zigong 643000, China
[c] College of Chemistry, Chongqing Normal University, Chongqing 401331, China
[d] Research Center for Carbon-Neutral Environmental & Energy Technology, Institute of Fundamental and Frontier Sciences, University of Electronic Science and Technology of China, Chengdu 611731, China
[e] Chongqing Polytechnic University of Electronic Technology, Chongqing 401331, China

ARTICLE INFO

Article history:
Received 7 May 2025
Revised 10 October 2025
Accepted 16 October 2025
Available online 17 October 2025

Keywords:
Hydrogen atom transfer
Nitrate reduction
Half-reaction regulation
Rapid-scan *in situ* FT-IR
Environmental photocatalysis

ABSTRACT

The efficient removal and conversion of nitrate (NO_3^-) from wastewater is an urgent environmental issue. The catalytic nitrate reduction reaction (NO_3RR) process, which involves transferring eight electrons and nine protons, poses significant challenges in improving hydrogen atom transfer (HAT). In this study, we synthesized $Bi_4O_5X_2$ (BOX, X = Cl, Br, I) nanosheets to enhance HAT efficiency by managing halogen vacancies and optimizing oxidation half-reactions. This approach significantly increased ammonia selectivity. We found that larger halogen radii and higher vacancy concentrations improve water dissociation, boosting HAT efficiency. Additionally, replacing the challenging water oxidation half-reaction with ethylene glycol (EG) oxidation aligned with NO_3^- reduction further improved HAT efficiency, achieving an NH_4^+ selectivity of 97.2 %. Rapid-scan *in situ* Fourier transform infrared (FT-IR) spectroscopy showed that iodine-rich vacancy surfaces accelerated the conversion of EG hydroxyl groups into carbonyls, releasing active hydrogen atoms and suppressing NO_2^- formation. This process efficiently converted nitrate to ammonia, presenting a promising method for photocatalytic NO_3RR pollutant resourcing. These findings offer valuable strategies for enhancing the production of reactive hydrogen atoms and effectively managing nitrate-nitrogen pollution.

© 2026 Published by Elsevier B.V. on behalf of Chinese Chemical Society and Institute of Materia Medica, Chinese Academy of Medical Sciences.

The nitrogen cycle is essential for sustaining the ecological balance between natural ecosystems and human activities [1–3]. However, human activities, such as excessive industrial wastewater discharge and overuse of nitrogen-based fertilizers, have disrupted this balance, causing eutrophication in aquatic ecosystems. This leads to the buildup of nitrates and nitrites in water, which can pose significant health risks [4]. As a result, efficiently removing nitrates from wastewater has become an urgent environmental concern [5]. Ammonia is particularly valuable for nitrate removal and resource recovery because of its importance in fertilizers and its use as a key raw material in the production of nitrogenous chemicals [6–11]. The primary method for ammonia production today is the Haber-Bosch process, which is energy-intensive and operates under harsh conditions, making it environmentally unsustainable [12,13]. Thus, finding alternative, energy-efficient, and eco-friendly methods for nitrate removal and ammonia production is a promising avenue for sustainable development [14,15].

The photocatalytic NO_3RR provides a sustainable method for transforming waste nitrates into valuable ammonia by utilizing renewable solar energy, which supports nitrogen cycle sustainability [16,17]. NO_3RR is a complex process that requires the transfer of eight electrons and nine protons ($NO_3^- + 8e^- + 9H^+ \rightarrow NH_3 + 3H_2O$) [18–21]. One key challenge in NO_3RR is the high demand for active hydrogen species (H^*) [22]. A shortage of H^* at catalytic sites can cause unwanted side reactions, decreasing nitrate conversion efficiency and ammonia selectivity. To enhance NO_3RR performance, in aqueous environment, it is essential to design catalysts that efficiently dissociate water at active sites to produce H^*, thus improving reaction efficiency and overall chemical activity [23–25]. The surface of bismuth oxyhalide materials is capable of *in situ* construction of halogen vacancies under light illumination, and surface hydroxylation induced during the construction of halogen vacancies is an effective scheme to enhance partial dis-

* Corresponding authors.
E-mail addresses: xadong@cqnu.edu.cn (X. Dong), pengyu@cqnu.edu.cn (P. Yu).

https://doi.org/10.1016/j.cclet.2025.111980
1001-8417/© 2026 Published by Elsevier B.V. on behalf of Chinese Chemical Society and Institute of Materia Medica, Chinese Academy of Medical Sciences.

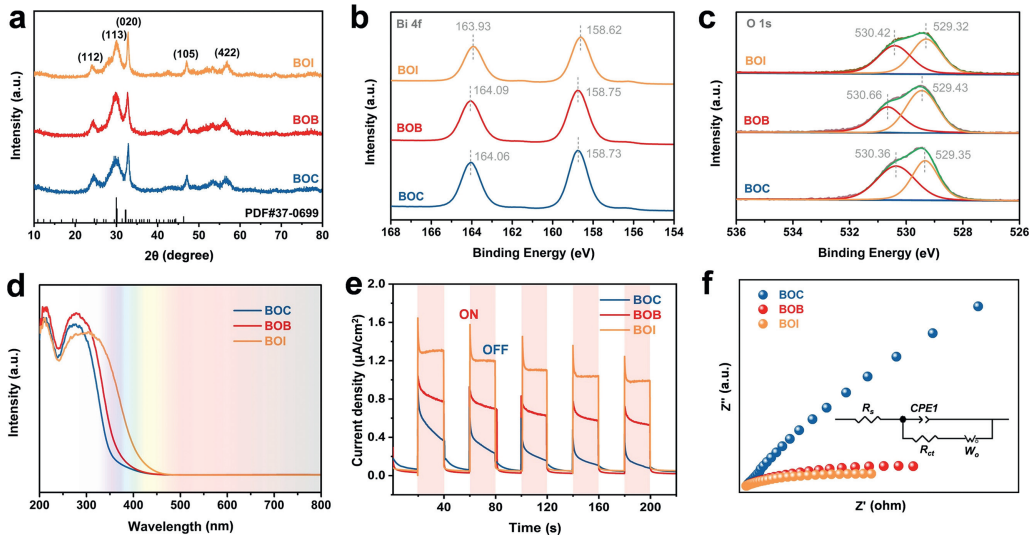


Fig. 1. Catalysts characterization and photo-electronic properties testing. (a) XRD pattern. Fitted XPS spectra of Bi 4f (b) and O 1s (c). (d) UV–vis diffuse reflection spectroscopy (DRS) spectra. Photocurrent (e) and EIS spectra (f) of BOC, BOB and BOI.

sociation of water molecules and improve HAT efficiency [26–28]. Therefore, rational regulation of the halogen vacancy construction process on the surface of bismuth oxyhalide materials will effectively enhance the HAT and improve the efficiency of ammonia synthesis.

The oxidation of water, acting as the oxidation half-reaction in the nitrate reduction process (NO_3RR), presents considerable challenges in producing reactive hydrogen species. The difficulties stem from two key factors [29]. First, although water deprotonation is easily achieved with an appropriate base ($pK_a = 15.74$), the high bond dissociation energy (BDE = 118 kcal/mol) and water's inherent thermodynamic stability make breaking the O–H bond especially challenging [30,31]. Second, after hydroxyl radicals ($^{\cdot}OH$) are formed, they cannot release another hydrogen atom without producing a highly reactive oxygen atom [32]. While halogen vacancies can enhance the HAT process, the challenges in the water oxidation half-reaction continue to limit NO_3RR efficiency. To address this issue, replacing water with more easily oxidized organic substrates in the oxidation half-reaction can significantly improve the process [20,33]. This strategy would improve HAT efficiency and, in turn, boost ammonia production in NO_3RR.

In this study, we synthesized BOX nanosheets to explore how photoinduced halogen vacancies of varying atomic sizes affect HAT efficiency and NO_3RR performance. By creating dynamic halogen vacancies, we facilitated the partial dissociation of water molecules, producing reactive hydrogen atoms. The efficiency of this process increased with larger halogen atomic radii. Additionally, replacing water oxidation with more easily oxidized organic compounds further boosted HAT efficiency. *In situ* FT-IR spectroscopy in aqueous solution showed that when ethylene glycol (EG) replaced water in the oxidation half-reaction, surfaces with I vacancies efficiently promoted the conversion of EG's hydroxyl groups to carbonyls, releasing a significant amount of reactive hydrogen atoms. This reaction reduced the formation of nitrite (NO_2^-) as a byproduct, enhancing both conversion rates and the selectivity of the photocatalytic NO_3RR. This study clarifies the principles of dynamically controlling halogen vacancy concentration and shows that adjusting the oxidation half-reaction greatly improves HAT efficiency. These findings not only advance ammonia synthesis through NO_3RR but also provide valuable insights for designing functional materials that efficiently supply reactive hydrogen atoms for chemical synthesis.

The crystalline phases of BOC, BOB, and BOI were analyzed using XRD (Fig. 1a), all the diffraction peaks of the BOB in XRD patterns can be assigned to monoclinic $Bi_4O_5Br_2$ phase (space group $P2_1$), corresponding to the PDF card #37-0699. In order to compare the effect of different halogen vacancy configuration differences on the HAT effect, the synthesized BOC and BOI were synthesized by keeping the same synthesis conditions as much as possible, and only replacing KBr with KCl or KI, and the synthesized materials were consistent with BOB in crystal structure from the XRD results [26,27,34]. XPS measurements were conducted to examine the surface structures of the synthesized samples. Fig. 1b presents the Bi 4f XPS spectra for the three samples. The Bi 4f spectra in Fig. 1b display two prominent peaks, corresponding to the $4f_{7/2}$ and $4f_{5/2}$ electrons of Bi^{3+}. The Bi 4f peak of BOI shifts significantly towards lower binding energy compared to BOC and BOB, indicating that Bi gains more electrons and slightly reduces its chemical valence as the halogen atom radius increases. In the O 1s XPS spectra (Fig. 1c), the characteristic peaks correspond to lattice oxygen atoms near the surface (~529.4 eV) and surface oxygen (~530.5 eV) [35]. A slight shift towards higher binding energies is observed for the surface oxygen in BOB compared to BOC and BOI, suggesting a change in the local chemical environment on the BOB sample's surface (Figs. S2-S4 in Supporting information). In addition, no obvious N 1s XPS peaks were detected (Fig. S5 in Supporting information), proving that the oleylamine was thoroughly removed during the synthesis process.

The absorbance properties of the BOX samples were evaluated using UV–vis diffuse reflectance spectroscopy (UV–vis DRS). As shown in Fig. 1d and Fig. S6 (Supporting information), the UV–vis DRS results show that the absorption band edges of BOC, BOB, and BOI are red-shifted sequentially, indicating improved light absorption as the halogen atom radius increases. Several characterization techniques were employed to examine the efficiency of photogenerated carrier separation. In order to further investigate the separation efficiency of the photogenerated electron-hole pairs of the materials, transient photocurrent experiments under Xe lamp illumination were performed on three samples. In general, the higher the separation efficiency of the photogenerated electron-hole pairs, the stronger the photocurrent. Fig. 1e shows that the transient photocurrent of BOI is stronger than that of BOB as well as BOC, which may be due to the narrower bandgap width of BOI that promotes the photogenerated charge separation [36,37]. The Nyquist

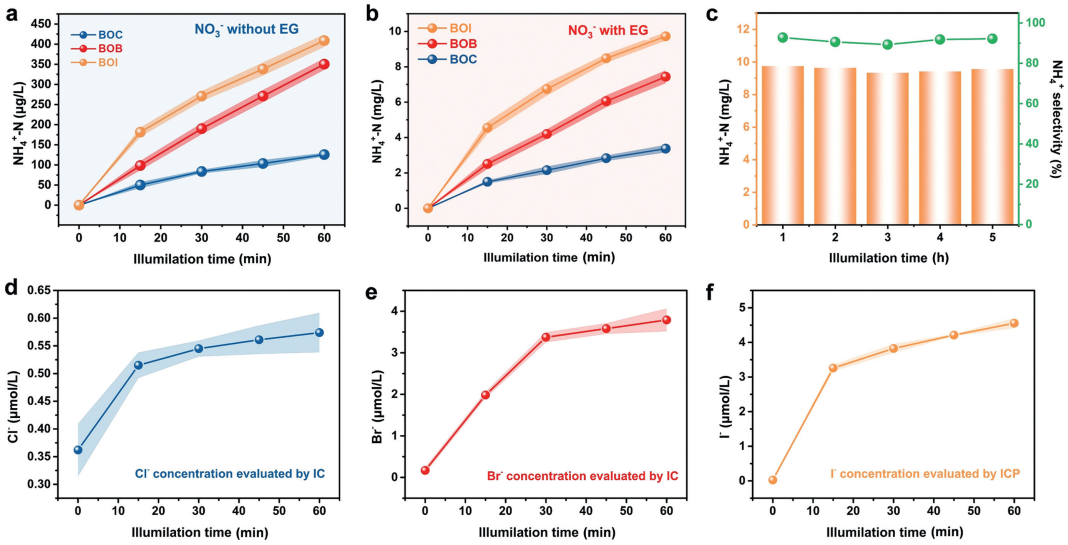


Fig. 2. Photocatalytic efficiency test. (a, b) Photocatalytic activity of the as-synthesized samples for the yield of NH_3 under NO_3^- solution without (a) and with (b) EG. (c) Cycle photocatalytic performance of BOI. (d-f) Quantitative determination of Cl^- (d), Br^- (e) and I^- (f) concentration in the aqueous solution.

plots acquired from electrochemical impedance spectroscopy (EIS, Fig. 1f) manifest the smallest arc radius of BOI with lowest charge transfer resistance and fastest charge transfer rate [38]. To obtain a quantitative result, the equivalent circuit was fitted and presented as an inset in Fig. 1f, and the corresponding fitting consequences were summarized in Table S3 (Supporting information). R_s is considered as the resistance of the glassy carbon electrode-catalyst interface. Apparently, the gap between the fitted R_s values for different photocatalysts does not differ much, indicating that the electrical contact at the glassy carbon electrode-catalyst interface is relatively tight for all photocatalysts. R_{ct} represents the charge transfer impedance generated during the catalytic reaction and is an important parameter for analyzing the catalytic activity of different catalytic materials. The charge transfer resistance values of BOC, BOB, and BOI are 16.84, 0.76, and 0.29 kΩ, respectively. BOI has a lower charge transfer resistance than BOC and BOB signifying an efficient charge transport in the nanocomposite photocatalyst, which also makes it easier for I in BOI to obtain electrons to *in situ* build I vacancies under light illumination and further promotes efficient NO_3^-RR reaction.

After analyzing the structural and absorptive properties of BOX, the samples were further examined through a photocatalytic nitrate reduction test. BOI demonstrated notable photocatalytic activity in ammonia synthesis *via* nitrate reduction, using H_2O as the proton donor under Xe lamp illumination. NH_4^+ concentration was measured using ion chromatography (IC). Although halogen vacancies can promote partial H_2O dissociation and facilitate the HAT process, the BOX sample still showed a low NO_3^- to ammonia conversion rate in pure aqueous conditions (Fig. 2a, NH_4^+-N of the order of μg/L). To enhance active proton concentration, 1 mL of ethylene glycol was added to the reaction precursor to replace the H_2O oxidation half-reaction, which substantially increased the ammonia conversion (Fig. 2b, NH_4^+-N to the order of mg/L). After 1 h of illumination, BOI achieved an NH_4^+ yield of 3.47 ± 0.09 mmol $g_{cat.}^{-1}$ h^{-1}, surpassing BOB (2.66 ± 0.13 mmol $g_{cat.}^{-1}$ h^{-1}) and significantly exceeding BOC (1.21 ± 0.08 mmol $g_{cat.}^{-1}$ h^{-1}). In addition, the quantum efficiencies of photocatalytic NO_3^-RR of the BOI in the EG-free solution as well as EG solution were also calculated, which were 0.01 % and 0.24 %, respectively, demonstrating that the addition of EG can substantially enhance the proton transfer efficiency and the utilization of light has been greatly improved. The catalytic stability of BOI was evaluated through five consecutive cycles (Fig. 2c and Fig. S9 in Supporting information), where it consistently maintained a high NO_3^- removal rate (~90 %), demonstrating excellent long-term stability. In the oxidative half-reaction of ethylene glycol, the formation of formic acid (Fig. S10 in Supporting information) resulted in the faster release of higher concentrations of active hydrogen compared to H_2O. This enhancement significantly improved both the conversion rate and selectivity of NH_4^+. In order to verify whether the nitrogen source of the generated NH_3 is derived from NO_3^-, isotope labeling experiments were performed for BOI. As shown in Fig. S19 (Supporting information), triple $^{14}NH_4^+$ and double $^{15}NH_4^+$ signals were detected in the NMR spectra using $^{14}NO_3^-$ and $^{15}NO_3^-$ as the reaction substrates, verifying that the reactant NO_3^- was reduced to NH_4^+ as expected.

The concentrations of Cl^- (Fig. 2d) and Br^- ions (Fig. 2e) in the aqueous phase were measured using anion chromatography (IC), while I^- ions (Fig. 2f) were analyzed by inductively coupled plasma (ICP-AES). After 1 h of illumination, the concentrations of chloride, bromide, and iodide ions were 0.21 ± 0.03, 3.79 ± 0.27, and 4.56 ± 0.14 μmol/L, respectively. The increasing concentrations of halogen ions from BOC, BOB, and BOI indicate that larger halogen atoms are more prone to precipitation, leading to higher halogen vacancy concentrations on the photocatalyst surfaces, which also matches the morphological structure of the series photocatalysts, in which the strain on the nanotube surface effectively enhances the rate of I vacancies construction. The surface halogen vacancy concentrations of BOC, BOB, and BOI were estimated to be 0.09 % ClV, 0.61 % BrV, and 0.81 % IV, based on the halogen ion concentrations in the aqueous solution. A clear correlation was established between halogen vacancy concentration and the NO_3^- photoreduction efficiency in ammonia synthesis. Importantly, the samples after the construction of halogen vacancies after light illumination were able to spontaneously regenerate in an aerobic environment, showing good structural stability (Fig. S20 in Supporting information).

To better understand the mechanisms behind improving nitrate-to-ammonia conversion and selectivity by adjusting HAT efficiency, solid-state and *in situ* liquid electron paramagnetic resonance (EPR) experiments were conducted to analyze the radicals formed during NO_3RR and their role in the reaction. The solid EPR signals of BOC, BOB, and BOI under illumination are shown in Fig. 3a. After 10 min of illumination, the signals at $g = 2.002$ increased for all three samples, indicating the formation of surface

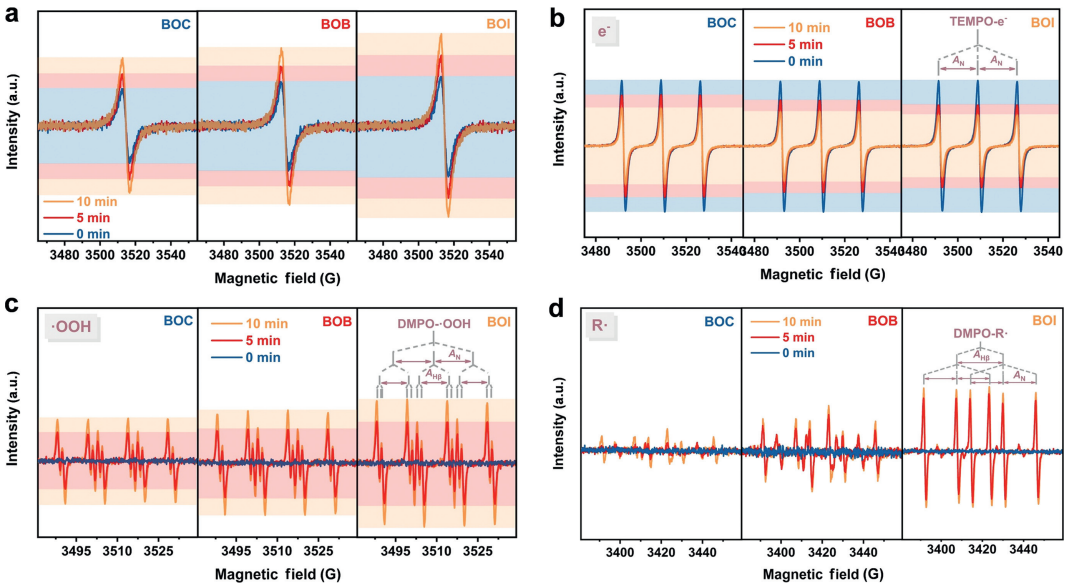


Fig. 3. The generation of reactive radicals during the photocatalytic redox reactions. (a) EPR spectra of as-synthesized samples in darkness and with Xe light illumination for 10 min under N_2 atmosphere at room temperature. (b) ESR spectra of variation of e^- captured by TEMPO with Xe light illumination for 10 min. ESR spectra of ^-OOH (c) and R^- (d) radicals captured by DMPO with Xe light illumination for 10 min.

vacancies. This corresponds with the increased halogen concentrations in the solution, with BOI showing the highest vacancy concentration. TEMPO was then used as a trapping agent to detect the production and behavior of photogenerated electrons (e^-, Fig. 3b). The interaction between e^- and NO_3^- in BOC, BOB, and BOI under light illumination showed that higher concentrations of dynamic vacancies lead to different levels of e^--h^+ utilization during the photocatalytic NO_3RR process.

Increased utilization of photogenerated electrons is expected to enhance oxidation half-reactions, thereby facilitating HAT. Initially, we confirmed the water oxidation half-reaction in a pure aqueous NO_3^- solution without EG, to identify the radicals formed during water dissociation. 5,5-Dimethyl-1-pyrroline *N*-oxide (DMPO) was used as a spin trap in a 1 vol% water-dioxane solution (Fig. 3c). BOI exhibited an intense and complex multiplet signal, attributed to the DMPO-^-OOH adduct [39]. The ^-OOH radicals likely form from the recombination of the highest concentration of ^-OH radicals on the BOI surface [40], occurring alongside the creation of *in situ* photoinduced I vacancies and enhanced water ionization. Notably, the BOI surface generates more ^-OOH radicals, indicating that increased vacancy concentration further promotes partial water dehydrogenation after surface vacancy construction is complete. Specifically, adding EG to the reactants resulted in considerable ^-R radical generation (Fig. 3d), with BOI yielding the highest amount of these radicals. This indicates that the high concentration of I vacancies enhances the dehydrogenation of EG during the reaction, which greatly aids in the transfer of hydrogen atoms and the reduction of NO_3^-. The solid ESR results, along with radical trapping experiments, demonstrated that the rapid construction of high-concentration halogen vacancies directly enhances HAT efficiency. Furthermore, substituting the oxidative half-reaction from water oxidation to the more easily executed organic oxidation further boosts HAT efficiency, ultimately improving ammonia synthesis *via* NO_3^- reduction.

The mechanism of hydrogen atom extraction from pure water and EG during the NO_3RR process was investigated using *in situ* FT-IR spectroscopy under chopper irradiation. The chopper irradiation process was synchronized with the *in situ* FT-IR measurements, as depicted in Fig. S22 (Supporting information). After 20 min of vacuum treatment, a drop of NO_3^- solution (either pure aqueous or containing EG) was placed on the BOI film surface. Approximately 0.2 MPa of Ar pressure was applied to conduct the *in situ* FT-IR test (Scheme S2 in Supporting information). In Figs. 4a–c (pure NO_3^- solution) and Figs. 4d–f (NO_3^- solution with EG), irradiation by a 355 nm laser produced a featureless background absorbance, increasing steadily between 1200 and 3600 cm^{-1} and intensifying with prolonged exposure.

In a pure NO_3^- solution without EG, characteristic vibrations are observed: O–NO_2 asymmetric stretching for NO_3^- at 1609 cm^{-1} [41], antisymmetric stretching vibration of the NO_2 group from the chelated nitro configuration at 1298 cm^{-1}, N=O stretching for NO_2^- at 1376 cm^{-1} [41], and N–H asymmetric deformation for the final product NH_4^+ at 1474 cm^{-1} [42,43]. After adding EG, the same characteristic peaks were observed, along with a broad peak near 3050 cm^{-1}, attributed to N–H stretching of NH_4^+ [44,45]. The increased intensity of this peak confirms a higher concentration of NH_4^+ was produced. Furthermore, it is evident that the peak at 1554 cm^{-1} can be attributed to the carbonyl groups, verifying the dehydrogenation of ethylene glycol and its further conversion to formic acid.

The normalized absorption intensities for NO_3^-, NO_2^-, and NH_4^+ vibrations are shown in Figs. 4g–i. With the addition of EG, the absorption intensities of NO_3^-, NO_2^-, and NH_4^+ increased over time, particularly for NO_3^-. This suggests that EG not only avoided competing with NO_3^- for surface adsorption sites but also enhanced NO_3^- adsorption on the catalyst. Notably, the increased NO_3^- adsorption did not result in higher NO_2^- production. Instead, it accelerated NO_3^- reduction directly to NH_4^+. This indicates that EG facilitates hydrogen atom transfer, improving NO_3^- reduction efficiency for ammonia synthesis.

In summary, NO_3^- is a ubiquitous pollutant in industrial and agricultural wastewater, and value-added photocatalytic reduction of NO_3^- to NH_3 can provide sustainable energy, economic and environmental benefits. This work provides insights into the role of enhancing photocatalytic HAT efficiency for NO_3RR. The *in situ* construction of halogen vacancies on the surface of BOX promotes the partial dissociation of H_2O in the aqueous system, generating active hydrogen atoms to participate in the reduction half-reaction NO_3RR, and further replacing the aqueous oxidation half-reaction with the more readily carried out glycol oxidation enhances the

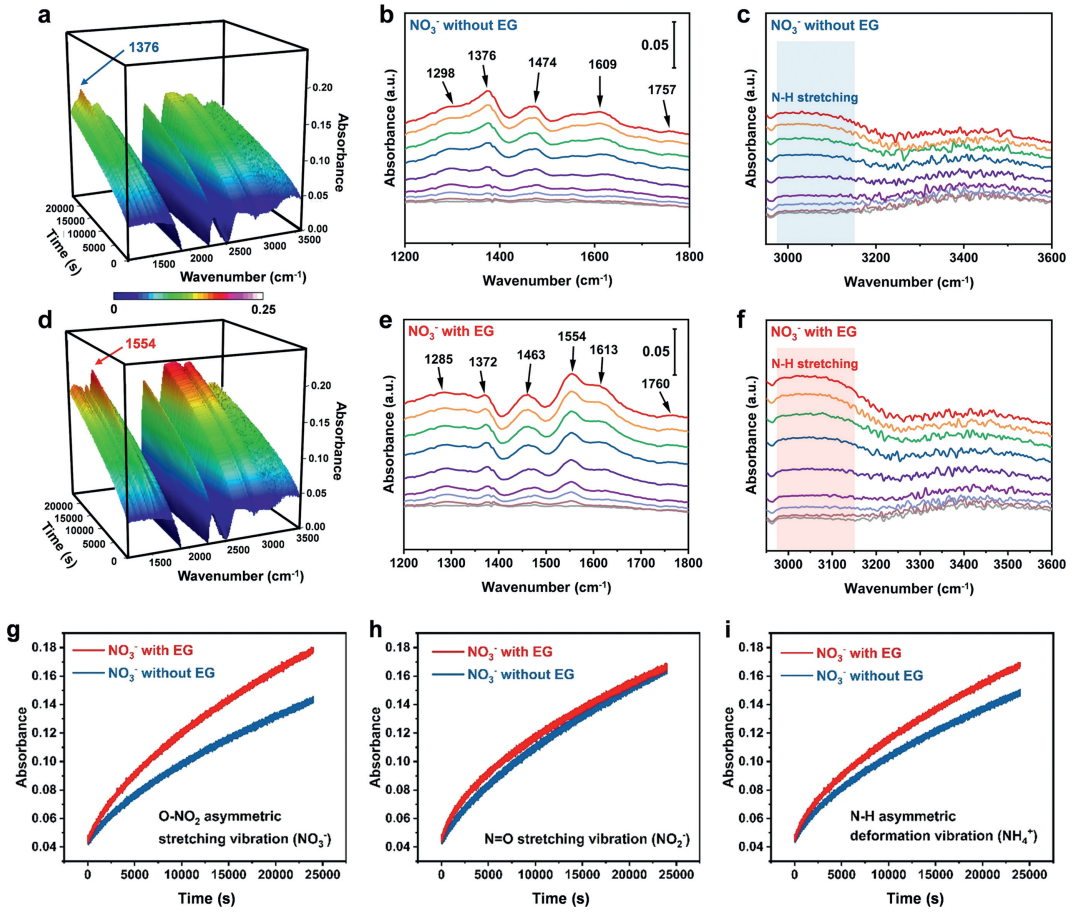


Fig. 4. Mechanistic analysis of photocatalytic NO_3^- reduction for ammonia synthesis. 3D spectral evolution process of the photocatalytic NO_3^- reduction process on BOI under NO_3^- solution without (a) and with (d) EG during all 100 irradiation cycles (0–2300 s). *In situ* FT-IR spectra of the photocatalytic NO_3^- reduction process on BOI under NO_3^- solution without (b, c) and with (e, f) EG recorded during irradiation cycles of 1, 2, 4, 8, 20, 40, 60, 70, and 100 (bottom to top). Evolution of peak normalized intensities of O–NO_2 asymmetric stretching vibration (g), N=O stretching vibration (h) and N–H asymmetric deformation vibration (i).

generation of active hydrogen atoms and significantly improves the efficiency of NO_3RR. Rapid-scan *in situ* FT-IR analysis confirmed that the replacement of water oxidation with ethylene glycol oxidation on the I-vacancy-rich surface accelerated the oxidation of hydroxyl groups to carbonyl groups, releasing a large number of reactive hydrogen atoms. This process inhibited the formation of the intermediate NO_2^- and improved the conversion and selectivity of photocatalytic reduction of NO_3^-. This work provides new insights and guidance for accelerating NO_3^- purification or value-added conversion by modulating HAT efficiency, and provides a new technological basis for the general application of more versatile photocatalytic systems in environmental and energy-related fields.

Declaration of competing interest

The authors declare that they have no known competing financial interests or personal relationships that could have appeared to influence the work reported in this paper.

CRediT authorship contribution statement

Fuqiang Guo: Writing – original draft, Visualization, Data curation. **Xian Shi:** Writing – review & editing, Data curation, Conceptualization. **Xing'an Dong:** Writing – review & editing, Writing – original draft, Visualization, Supervision, Funding acquisition, Formal analysis, Data curation, Conceptualization. **Chunyu Li:** Data curation. **Shanshan Xu:** Data curation. **Wendong Zhang:** Data curation. **Weidong Dai:** Data curation. **Wenjie He:** Funding acquisition, Data curation. **Xin Jin:** Data curation. **Peng Yu:** Writing – review & editing. **Fan Dong:** Writing – review & editing, Supervision, Funding acquisition, Conceptualization.

Acknowledgments

This work was supported by the National Natural Science Foundation of China (No. 22406014), the Natural Science Foundation of Chongqing (Nos. CSTB2025NSCQ-GPX0991, CSTB2024NSCQ-MSX1278), the Scientific and Technological Research Program of Chongqing Municipal Education Commission (Nos. KJQN202400512, KJZD-K202403102), the China Postdoctoral Science Foundation (No. 2023MD744137), the Foundation of Chongqing Normal University (No. 23XLB016) and the Sichuan Provincial Natural Science Foundation (No. 2025NSFTD0003). We also appreciate ceshihui (www.ceshihui.cn) for the TEM and XPS analysis.

Supplementary materials

Supplementary material associated with this article can be found, in the online version, at doi:10.1016/j.cclet.2025.111980.

References

[1] N. Lehnert, B.W. Musselman, L.C. Seefeldt, Chem. Soc. Rev. 50 (2021) 3640–3646.
[2] S. Han, H. Li, T. Li, et al., Nat. Catal. 6 (2023) 402–414.

[3] L. Fang, S. Wang, S. Lu, et al., Chin. Chem. Lett. 35 (2024) 108864.
[4] Y. Xiong, Y. Wang, J. Zhou, et al., Adv. Mater. 36 (2024) 2304021.
[5] L. Liu, S.J. Zheng, H. Chen, et al., Angew. Chem. Int. Ed. 63 (2024) e202316910.
[6] G. Qing, R. Ghazfar, S.T. Jackowski, et al., Chem. Rev. 120 (2020) 5437–5516.
[7] Y. Chen, X. Xia, L. Tian, et al., Chin. Chem. Lett. 35 (2024) 109789.
[8] J. Liang, Z. Li, L. Zhang, et al., Chem 9 (2023) 1768–1827.
[9] P.H. van Langevelde, I. Katsounaros, M.T. Koper, Joule 5 (2021) 290–294.
[10] Y. Mao, Y. Jiang, H. Liu, et al., Chin. Chem. Lett. 35 (2024) 108540.
[11] Y. Peng, G. Guo, S. Guo, et al., Angew. Chem. Int. Ed. 40 (2021) 22233–22240.
[12] H. Zhang, H. Wang, X. Cao, et al., Adv. Mater. 36 (2024) 2312746.
[13] F. Chen, Z. Wu, S. Gupta, et al., Nat. Nanotechnol. 17 (2022) 759–767.
[14] Y. Wei, J. Huang, H. Chen, et al., Adv. Mater. 36 (2024) 2404774.
[15] Y. Wang, Y. Yu, R. Jia, et al., Nat. Sci. Rev. 6 (2019) 730–738.
[16] H. Xu, Y. Ma, J. Chen, et al., Chem. Soc. Rev. 51 (2022) 2710–2758.
[17] Y. Li, C. Cheng, S. Han, et al., ACS Energy Lett. 7 (2022) 1187–1194.
[18] Y. Wang, C. Wang, M. Li, et al., Chem. Soc. Rev. 50 (2021) 6720–6733.
[19] K. Liu, H. Li, M. Xie, et al., J. Am. Chem. Soc. 146 (2024) 7779–7790.
[20] S. Shen, R. Chen, X. Li, et al., Environ. Sci. Technol. 58 (2024) 7653–7661.
[21] T. Zhao, W. Zhang, J. Xiong, et al., Separation Purif. Technol. 360 (2025) 130849.
[22] W. Liao, J. Wang, G. Ni, et al., Nat. Commun. 15 (2024) 1264.
[23] J. Wang, J. Cai, K. Ren, et al., Sci. Adv. 10 (2024) eadn7556.
[24] J. Yang, H. Qi, A. Li, et al., J. Am. Chem. Soc. 144 (2022) 12062–12071.
[25] Q. Gao, B. Yao, H.S. Pillai, et al., Nat. Synth. 2 (2023) 624–634.
[26] X. Dong, Z. Cui, X. Shi, et al., Angew. Chem. Int. Ed. 61 (2022) e202200937.
[27] X. Dong, X. Shi, Z. Cui, et al., ACS Nano 18 (2024) 9670–9677.
[28] X. Dong, K. Wang, Z. Cui, et al., Nano Res. 16 (2023) 6679–6686.
[29] G. Yang, P. Qiu, J. Xiong, et al., Chin. Chem. Lett. 33 (2022) 3709–3712.
[30] J.J. Warren, T.A. Tronic, J.M. Mayer, Chem. Rev. 110 (2010) 6961–7001.
[31] R.G. Agarwal, S.C. Coste, B.D. Groff, et al., Chem. Rev. 122 (2021) 1–49.
[32] B. Ruscic, A.F. Wagner, L.B. Harding, et al., J. Phys. Chem. A 106 (2002) 2727–2747.
[33] R. Chen, S. Shen, K. Wang, et al., Proc. Natl. Acad. Sci. U. S. A. 120 (2023) e2312550120.
[34] X. Shi, X. Dong, Y. He, et al., ACS Catal. 12 (2022) 3965–3973.
[35] X. Ma, L. Ma, S. Guo, et al., Angew. Chem. Int. Ed. 137 (2025) e202423157.
[36] W. Zhang, J. Xiong, S. Li, et al., Mol. Catal. 570 (2025) 114701.
[37] L. Wang, D. Lv, Z. Yue, et al., Nano Energy 57 (2019) 398–404.
[38] D. Kato, K. Hongo, R. Maezono, et al., J. Am. Chem. Soc. 139 (2017) 18725–18731.
[39] G.R. Buettner, Free Radic, Biol. Med. 3 (1987) 259–303.
[40] Y. Nosaka, A.Y. Nosaka, Chem. Rev. 117 (2017) 11302–11336.
[41] W.W. Simons, The Sadtler handbook of Infrared Spectra, Bio-Rad Laboratories, 1978.
[42] G. Zhang, C.D. Sewell, P. Zhang, et al., Nano Energy 71 (2020) 104645.
[43] Y. Zhao, Y. Zhao, G.I. Waterhouse, et al., Adv. Mater. 29 (2017) 1703828.
[44] J.R. Durig, C. Zheng, Vib. Spectrosc. 30 (2002) 59–67.
[45] C.C. Chuang, J.S. Shiu, J.L. Lin, Phys. Chem. Chem. Phys. 2 (2000) 2629–2633.